The total area of the bottom imaged by sidescan was 68.6 km^2, roughly 65 % of the total subaqueous area of the estuary between Burlington and New Castle, 80 % of the area below the 6-m isobath. Most of the remaining area (31.4 km^2) consists of shoals that were too shallow to be mapped without risking damage to the towed instrumentation. Though both sidescan sonar frequencies (100 and 500 kHz) were use to characterize the bottom, the backscatter mosaic was constructed from 100 kHz data because it provided more horizontal range.

5.2. Sidescan Backscatter

Because a detailed analysis of sidescan backscatter at the bedform scale was beyond the scope of this study, only the regional patterns are elaborated herein. The 12 backscatter mosaics are presented together in a large-scale map to illustrate the cumulative coverage (Figure 17; see Table 2 for details), and the individual 1-m resolution mosaics on which the sedimentary environments maps were based are presented as a composite GIS layer.

Table 2. Backcatter mosaic names and locations

DRBC Zone	Mosaic Name	Report Figure
5	New Castle	22
5	Christina	22, 23
5	Marcus Hook Bar	24
4–5	Marcus Hook	25, 26
4	Tinicum	26
4	Airport	27
4	Schuylkill	27, 28
3–4	Navy Yard	28
3	Camden	29
3	Petty Island	30
2–3	Palmyra	31
2	Burlington	32, 33

The spatial distribution of acoustic backscatter intensity exhibits a general along-estuary pattern that mirrors the predominant bed morphology and sediment type (Figure 17). For purposes of interpretation, backscatter intensity was divided into three categories: (1) *strong* (black to dark gray grayscale tones); (2) *moderate* (dark gray to light gray tones); and (3) *weak* (light grey to white tones). Backscatter intensity was

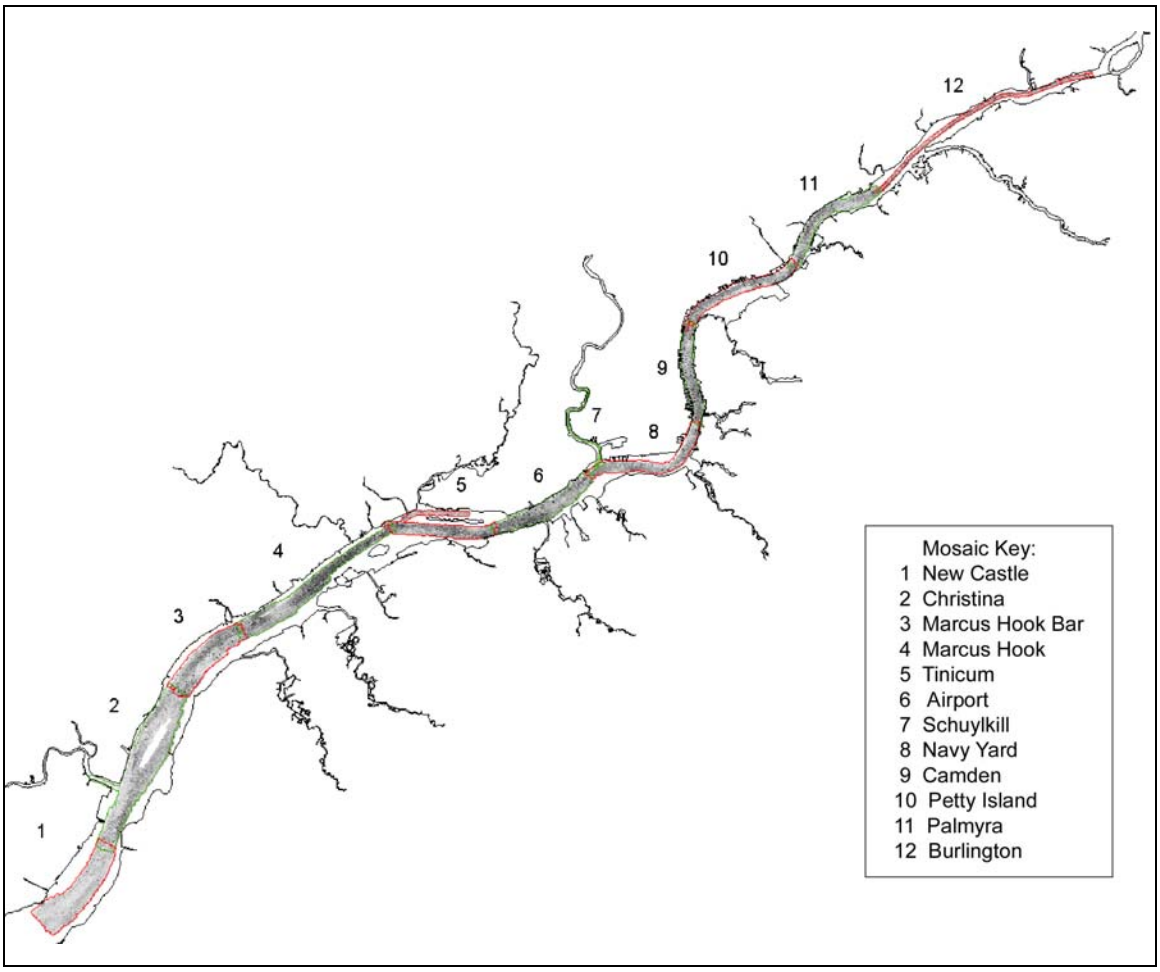

Figure 17. Sidescan sonar coverage map and acoustic backscatter distribution. See Table 2 for mosaic names and range. Interpreted versions of the 12 mosaics are presented in Figures 22–33.

moderate in Zones 2 and 3, moderate to strong in Zone 4, and weak in Zone 5, yet intra-zone variations spanning the full backscatter intensity spectrum were observed in places. Grain-size analysis confirmed that backscatter intensity generally increased with increasing grain size; however, sandy, rippled bottoms produced intensities that were equivalent to flat, gravelly bottoms. The strongest backscatter intensity was observed between Tinicum Island and Chester, most likely due an abundance of cobble and rock fragments present at the bed (Figure 17). In contrast, the lowest backscatter was observed just downriver off Marcus Hook, where a fluidized mud bottom was present. Backscatter intensity is uniformly weak downriver of the Marcus Hook Bar, consistent with the progressive increase in the mud content of the bed sediment. Further interpretation of the backscatter distribution is provided in Section 5.4.

5.3. Sediment Physical Properties

5.3.1. Porosity

Water content and porosity data are presented in Appendix D. As expected, the porosity of the subtidal estuary and marsh deposits varied with grain size among surficial (core top) samples, as well as with compaction, increasing with depth in the sediment column. Within 60 cm of the sediment-water interface, porosities ranged from 44 to 91 % with a mean of 73±0.09 % (1σ, n=310). As expected, sandy deposits exhibited lower initial (uncompacted) porosities than those of mud. The porosity of uniform muds decreased downcore by as much as 20–30 %, whereas grain-size variation modulated the downcore porosities of interbedded silts and clays (Figure 18).

5.3.2. Grain Size

Grain-size data (samples 1G–184G) were plotted in ternary charts to classify bottom types based on weight percentages of gravel, sand, mud, silt, and clay (Figure 19). Grain-size results for the lower estuary south of New Castle (samples 185G–298G) are not described here, though the data are tabulated in Appendix E. Bottom sediments of the upper estuary span the full range of sizes observed for river-estuaries in general, with all but three (gM, gmS, Z) of the 24 size classes represented (see Figure 4). For the gravel-sand-mud classification, gravel, sandy gravel, gravelly sand, and gravelly muddy sand were the most common gravel classes, whereas sand, muddy sand, sandy mud and mud characterized the majority of samples without gravel.

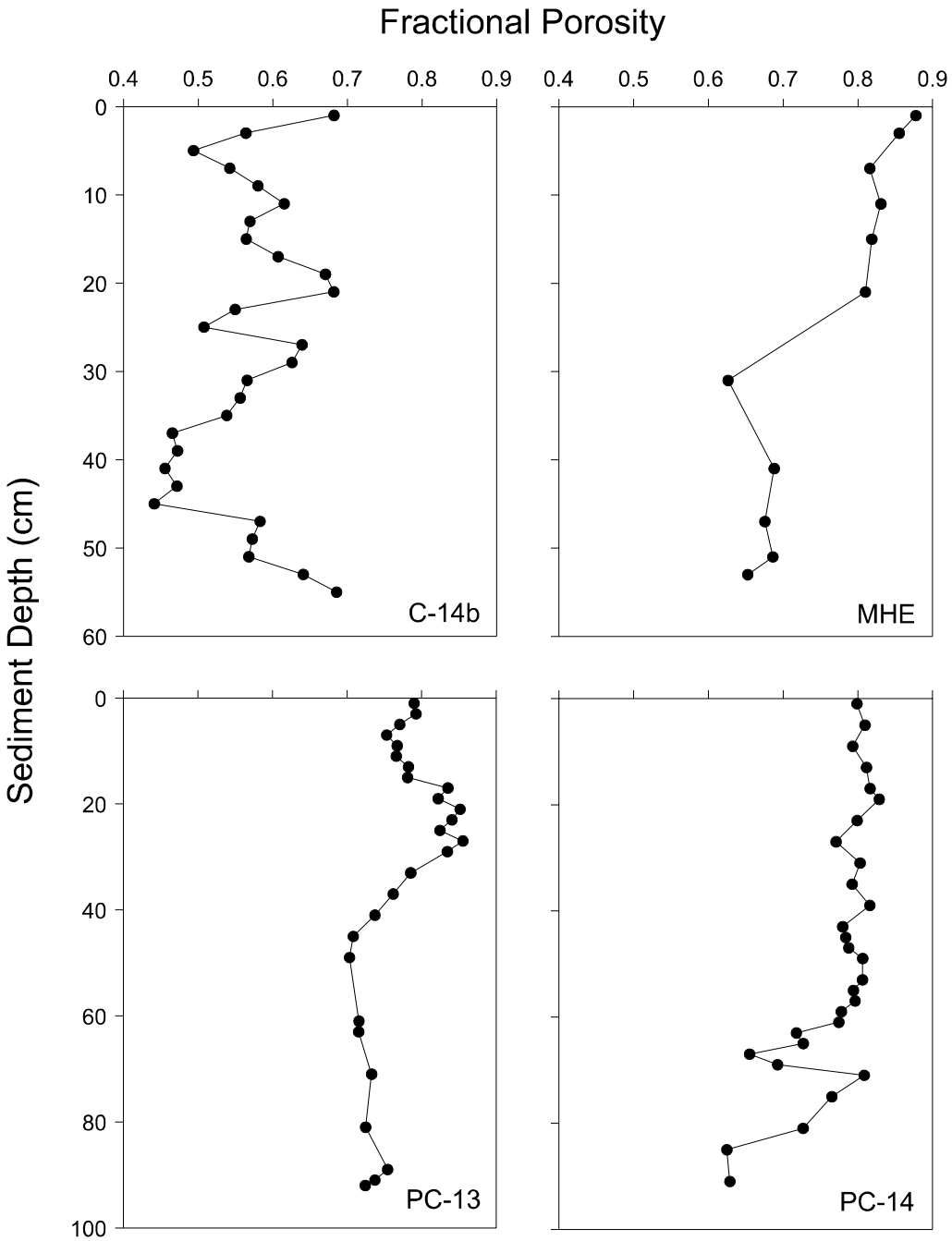

Figure 18. Downcore porosity profiles. Examples shown are from the estuary (C-14b, MHE) and tidal marsh sites (PC-13, PC-14). See Table 3 and Appendix C for locations.

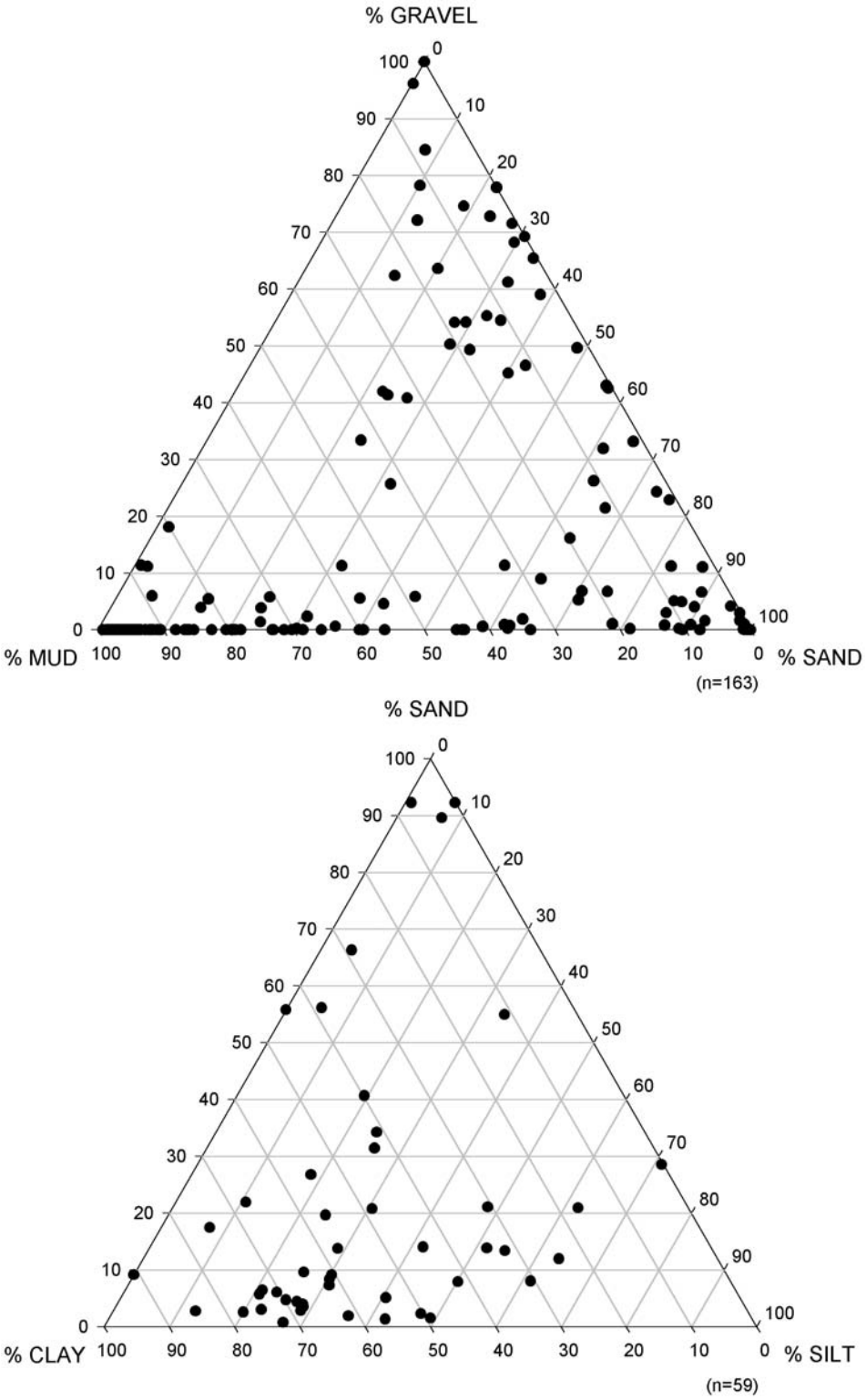

Figure 19. Results of grain-size analysis. Plotted are samples collected during cruise CH01-28. See Appendix E for tabulated data.

Silts and clays dominated the sand-silt-clay classification, with silty clay, clayey silt, sand clay, sandy silty clay, and clay being the most common classes. At grab-sampling sites 83G, 125G, and 131G, the bottom consisted of large cobbles and rock fragments that could not be recovered. Accordingly, a "rock" bottom type (R) not represented by the classification scheme is present in places. Lack of data clustering in the ternary plots indicates that distinct sedimentary provinces (i.e., facies) are not present within the natural channel (Figure 19), in other words, the sediment types are highly heterogeneous along the length surveyed and at the resolution of sampling.

In addition to spatial heterogeneity, temporal variability must be considered when interpreting the sediment-type distribution. For example, cores from the Rancocas River mouth and Marcus Hook shoal displayed a uniform layer of medium-grained sand atop interbedded, open-estuarine mud (Figure 20). This sedimentology implies a recent, abrupt increase in bottom energy manifested as a change from mud deposition in a shoal or mudflat setting (bottom of core) to bedload transport of sands derived from the estuarine channel or through shoreline erosion (core top). Another interpretation is that the supply of mud to these depositional sites has decreased through time such that sand has become predominant. Although the chronology and full nature of this change is unknown at present, it may be related to historical dredging disturbances and (or) shoreline stabilization works.

Along-estuary trends in sediment grain size were examined by plotting the weight percentages of gravel, sand, and mud as a function of axial position (Figure 21). Overall, the weight percentages of gravel varied by several orders of magnitude with no clear-cut trends, though a slight decrease around RM 75 in Zone 5 was indicated. The absolute weight percentages of sand generally decreased down-estuary from Zone 3 to Zone 5, but the cross-channel variability increased. In contrast, the across-channel variability in mud content decreased significantly along-estuary. The transition from a dominantly coarse-grained (sand and gravel) to fine-grained bottom (clayey silt to silty clay) occurs near the Zone 4–Zone 5 boundary, between RM 75 and RM 85. At least two factors may be

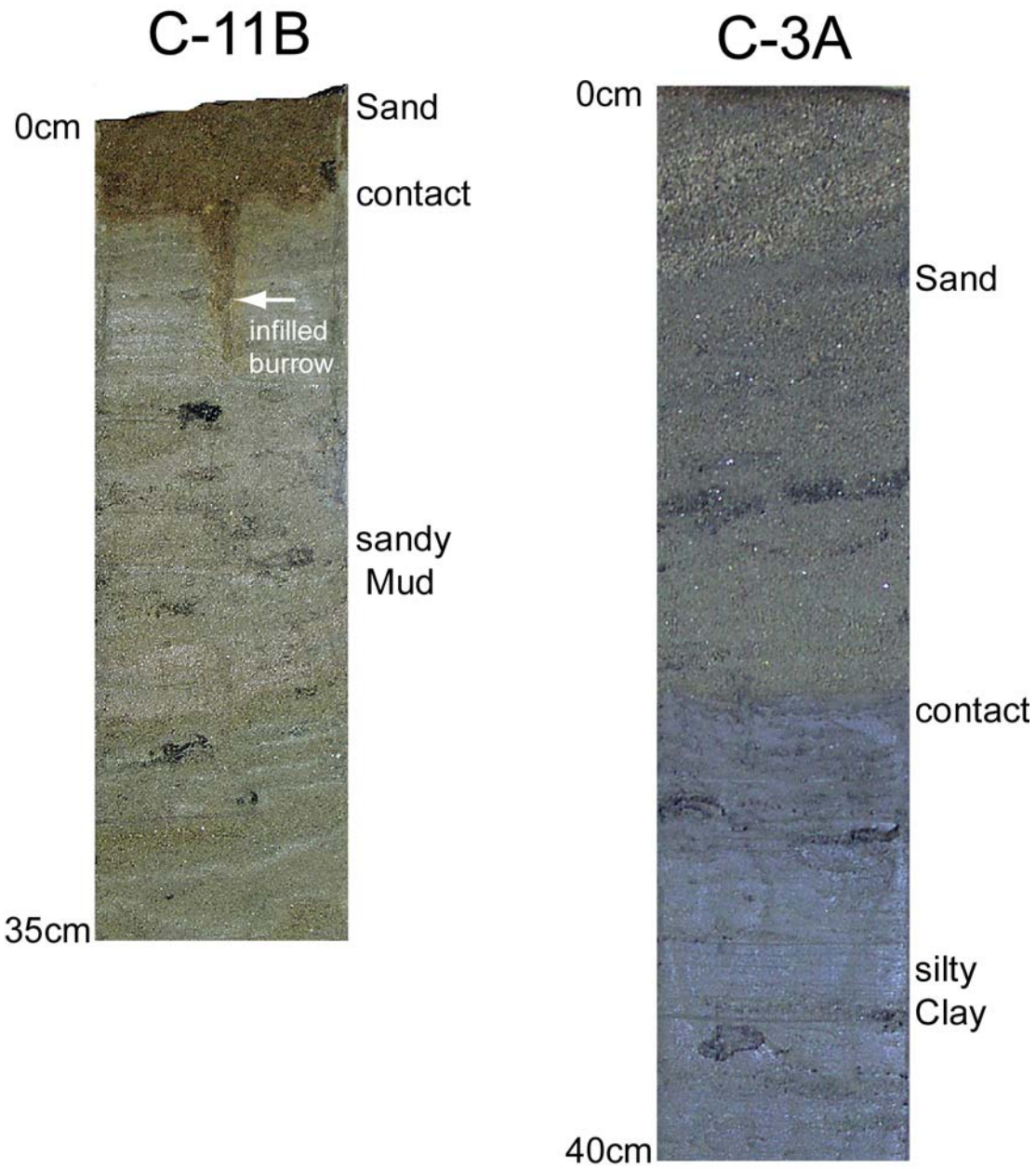

Figure 20. Photographs of cores C-3A and C-11B. See Figure 40 for location map and Appendix C for geographic coordinates. The sharp contact between sediment types marks a recent change from a fine-grained deposition to coarse-grained bed load environments.

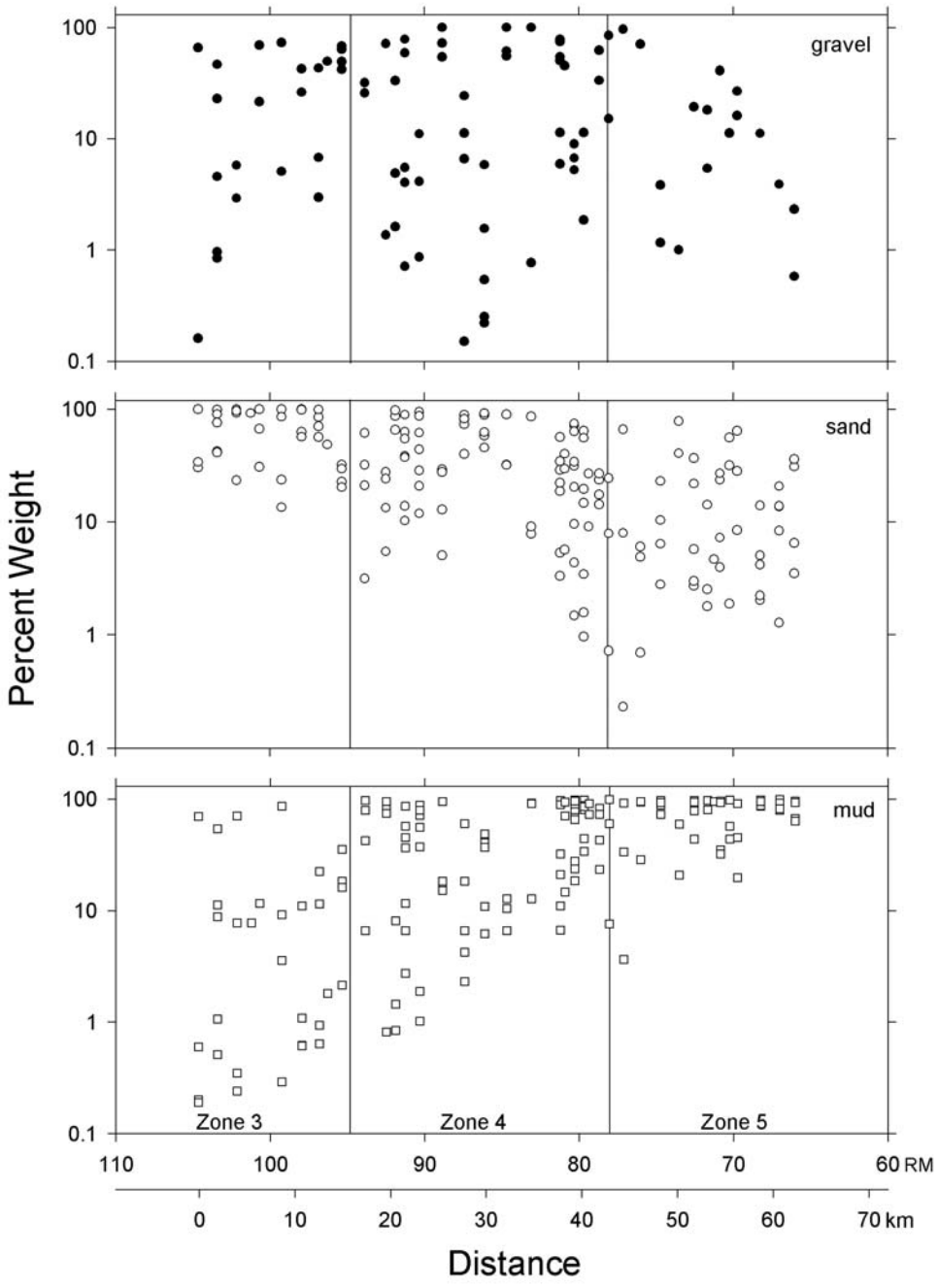

Figure 21. Plots of grain-size trends. Shown are grain-size analytical results for samples collected during cruise CH01-28 (see Appendix C for locations). Weight percentages are plotted versus distance in river miles from the bay mouth (0 RM) and kilometers relative to the first sampling transect. Corresponding DRBC Zones are noted for reference.

responsible for this transition. First, the estuarine channel widens rapidly from RM 100 to RM 80, perhaps reducing tidal-current velocities to below the level of competency for sand transport. Second, given that the head of the salinity intrusion typically falls within this region, flocculation and rapid deposition of particle aggregates locally may increase the mud content of the bed. Although general estuarine processes can be invoked to explain the Zone 4–5 sand-to-mud transition, the causal mechanisms cannot be ascertained from the grain-size data alone.

5.4. Sedimentary Environments

A map depicting the distribution of sedimentary environments in the study area was created from the sidescan sonar mosaic and grain-size data, using dominant sediment type and mode of transport (as suggested by bedforms) as the primary delimiters. The map was created by overlaying georeferenced bottom-type and backscatter-mosaic layers in GIS and tracing the backscatter patterns according to intensity (grayscale tone), surface relief (extent of acoustic shadowing), and local bottom type. In this report, the sedimentary environments map is subdivided into 12 smaller maps scaled at approximately four-by-four nautical miles (Figures 22–33) with geographic bounds identical to those of the sampling coverage maps (Figures 5–16). The full-scale map is presented as a layer in the GIS database.

Six types of sedimentary environments were identified following criteria modified from (Knebel et al., 1999): (1) fine-grained deposition; (2) coarse-grained bedload; (3) fine-grained reworking; (4) mixed-grain reworking; (5) coarse-grained reworking; (6) and non-deposition or erosion. Specific characteristics of these environments are elaborated below and summarized in Table 3.

Areas of fine-grained sediment deposition (mud) exhibit uniformly weak to very weak backscatter intensity generated by flat bottoms composed of high-porosity (>75%) or fluidized mud. The Marcus Hook anchorage and Christina River mouth region are examples of the fine-grained deposition environment (Figure 25). These bottoms are generally devoid of bedforms, with the exception of linear, sedimentary furrows observed in places. The radioisotope Be-7 was detected at one fine-grained site off Marcus Hook, suggesting that deposition within these environments is active on a seasonal basis (see Section 5.6.2.).